

Dynamics of capillary condensation in bistable optical superlattices

Zeno Gaburro, Mher Ghulinyan, and Lorenzo Pavesi

Nanoscience Laboratory, Department of Physics, University of Trento, via Sommarive 14, Povo, I-38050 Trento, Italy

Pierre Barthelemy, Costanza Toninelli, and Diederik Wiersma

European Laboratory for Nonlinear Spectroscopy and INFN-BEC, via Nello Carrara 1, Sesto Fiorentino, 50019 Florence, Italy

(Received 1 October 2007; revised manuscript received 7 February 2008; published 27 March 2008)

The optical transmission through a porous superlattice is modulated by capillary condensation and evaporation of ethanol. The system exhibits optical bistability, with the two stable states characterized by a different amount of liquid ethanol in the pores. Switching between states is controlled by the input power of the incident light beam. By tuning the input power at various speeds, we study the dynamics of condensation and evaporation and study the behavior of the hysteresis and switching thresholds. We find that the time response of the system is limited by the condensation process, which is faster in pores with lower radius. We also report on the dependence of the hysteresis loop on vapor concentration.

DOI: [10.1103/PhysRevB.77.115354](https://doi.org/10.1103/PhysRevB.77.115354)

PACS number(s): 78.20.Nv, 42.65.Pc, 42.70.Qs, 47.56.+r

I. INTRODUCTION

The optical response of photonic crystals (PCs) depends not only on material properties but also on the structure itself and, therefore, can be designed with large flexibility. Photonic crystals are a viable material to attain light confinement at the scale of wavelength or below, which is an intriguing perspective for the realization of devices for integrated photonic circuits.^{1,2} Several effects have been proposed to achieve tunability in PCs, for example by using the temperature dependence of the plasma frequency of semiconductors,³ the infiltration of liquid crystals and subsequent control of their orientation by external electric fields or temperature,^{4,5} the dependence of electric permittivity or magnetic permeability on externally applied electric or magnetic fields,⁶ or dependence on temperature and magnetic fields in superconducting photonic crystals.⁷⁻⁹

Photonic materials fabricated from porous structures allow for an interesting alternative approach to modulate their optical properties, namely, by exposure to vapors. With appropriately chosen design parameters, the vapor molecules adsorb on pore walls, and their accumulation induces the formation of a liquid phase in pores whose cross section is smaller than a critical value. The substitution of air with liquid changes the average refractive index and thereby the optical response of the system. In the case of cylindrical pores open at both ends, this critical size can be expressed as a radius r_c , which depends on the temperature T and the vapor pressure P according to a modified Kelvin equation¹⁰

$$r_c = \frac{v_m \gamma}{k_B T \ln(P_0/P)}, \quad (1)$$

where P_0 is the saturation pressure, v_m is the adsorbate molecular volume, and γ is its surface tension.

If the size of the pores is well below the optical wavelength, the system can be described to first approximation as a homogeneous material, whose effective dielectric function ϵ_{eff} (or, equivalently, its effective refractive index n_{eff}) is a suitably weighted average of the dielectric functions of the solid matrix and of the pores (for example, see Ref. 11 for a

review). A commonly assumed approximation is the one introduced by Bruggeman,¹² which is the one adopted in our calculations. Since the index of the pores can be modulated by condensing and evaporating liquid phases, the effective refractive index of these porous materials is also modulated. In porous silicon layers, this modulation effect has been first observed in 1996.¹³ An example of its application is that of the modulation of optical Fabry–Pérot microcavities.¹⁴ An important characteristic of this modulation mechanism is that, with suitable choice of vapor, the relative modulation can be quite large ($\Delta n/n \approx 10^{-2}$),¹⁶ as compared to what is attainable with other physical effects.^{17,18} Thus, a large nonlinear optical response can be achieved even by small modulation of any physical quantity on the right hand side of Eq. (1), which controls the amount of the liquid phase.

An interesting case of tunable response is the modulation of the optical properties using the light signal itself. If one relies on the intrinsic nonlinear properties of materials, a large intensity is usually required because the nonlinear coefficients are generally small. In this context, the photonic effects can become particularly interesting. For example, light confinement and slow group velocity—as observable in the proximity of band edge states of photonic crystals—can increase the local intensity by several orders of magnitude and enhance the efficiency of the nonlinearity.¹⁹⁻²² This strategy can also be applied to optical modulation based on capillary condensation, namely, by concentrating light in selected regions of structured photonic porous samples. This way, the presence of the liquid phase can be modulated by thermal evaporation with very low input intensities. Recently, we have followed this strategy to achieve optical bistability in an optical Zener tunneling (ZT) device, fabricated as a one-dimensional multilayer structure of porous silicon.²³

II. SAMPLE DESIGN

An optical ZT device is an optical superlattice with transmission minibands that can be tuned in and out of resonance.²⁴ Optical minibands can be achieved by building a stack of coupled Fabry–Pérot microcavities. In an optical

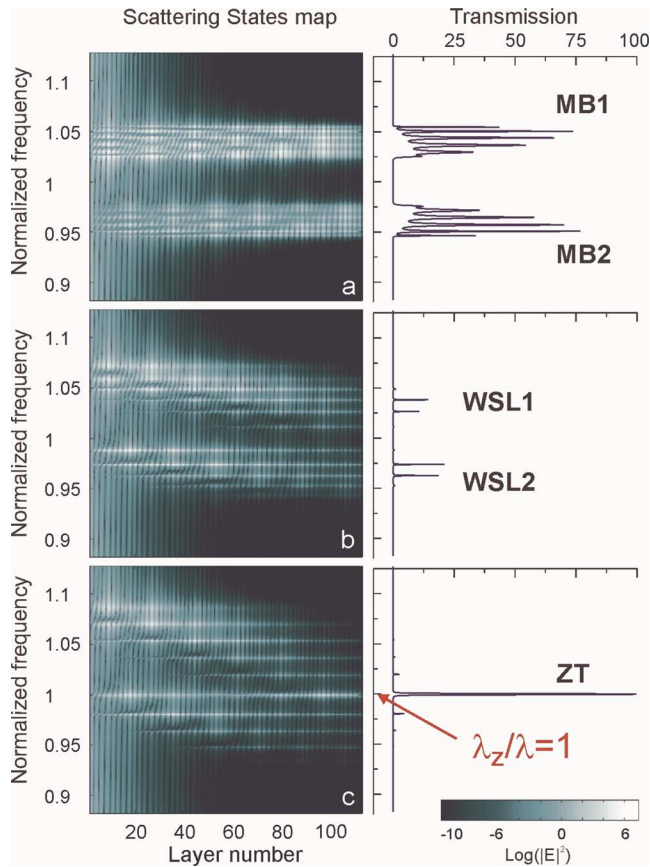


FIG. 1. (Color online) Calculated distribution of light intensity (scattering state maps, left column) and transmission spectra (right column) of typical porous silicon Zener tunneling (ZT) structures. The intensity is plotted as a color scale versus the normalized frequency ω/ω_z and depth inside the sample, where $\omega_z = 2\pi c/\lambda_z$ is the (arbitrary) frequency at which ZT occurs. In the absence of a refractive index gradient, two flat minibands MB1 and MB2 are formed, separated by (a) a minigap. The introduction of a gradient in the refractive index tilts the photonic bands of the superlattice, and (b) optical Wannier–Stark ladders (WSLs) appear. At a critical gradient value, a resonant coupling between the last state of MB1 and the first one of MB2 occurs. Coupling induced delocalization of these states takes place, which appears as an (c) intense resonant tunneling channel and an enhanced ZT transmission peak (Ref. 24).

ZT system, two or more minibands are realized by alternating, in the multilayer stack, two different types of microcavities (the difference being in the microcavity resonance frequency). A gradient is introduced along the propagation direction to create Wannier–Stark ladders in the minibands, which couple at a critical value of the gradient leading to optical Zener tunneling. The calculated distribution of the intensity and the transmission spectra of three porous silicon superlattices with two minibands and different gradients (0%, 6.7%, and 10.3%) are shown in Fig. 1. The Zener tunneling condition is achieved in Fig. 1(c).

In Ref. 23, we have experimentally demonstrated optical bistability in such a structure by modulating the condensation condition via the intensity. The effect is explained in Fig. 2.

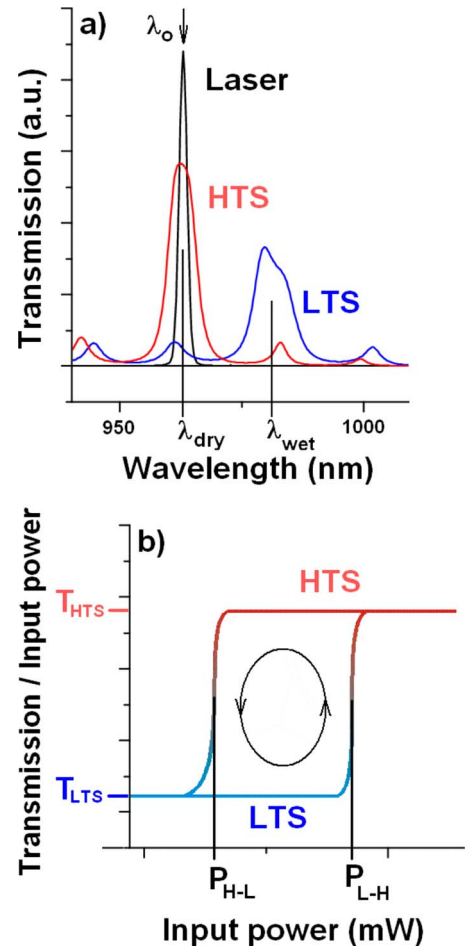


FIG. 2. (Color online) (a) Simulation of the two transmission states of a bistable Zener structure. Spectrum of laser input is also shown (central wavelength = λ_o). The high transmission state (HTS) is centered at λ_{dry} , whereas the low transmission state (LTS) is centered at λ_{wet} . (b) Qualitative cartoon of ideal resulting hysteresis of the transmission coefficient evaluated at λ_o (T_{HTS} and T_{LTS} are, respectively, the values in HTS and LTS). P_{L-H} and P_{H-L} are the switching thresholds, as discussed in the text.

We have fabricated our samples centered at wavelength λ_z in their optical transmission spectra. Once these porous samples are fabricated, λ_z can be modulated by filling and emptying the pores with liquid. Insertion of liquid always causes a shift of the spectrum toward longer wavelength because the optical paths inside the photonic structure increase with increasing the refractive index. Therefore, spectra can be shifted from their “dry state” ($\lambda_z = \lambda_{dry}$), i.e., the state with empty pores, to a “wet state” ($\lambda_z = \lambda_{wet} > \lambda_{dry}$), a state with pores containing condensed liquid. As infiltrating fluid, we have used ethanol vapors for convenience and for their non-toxicity. The exposure to vapors can be controlled by adjusting the composition and pressure, and the resulting shift $\lambda_{wet} - \lambda_{dry}$ monotonically depends on the amount of the liquid phase inside the pores. In the following, we intend for λ_{dry} and λ_{wet} to be fixed wavelengths: in particular, the latter is fixed once we have set all the parameters at the right hand side of Eq. (1), i.e., the material parameters v_m and γ , the vapor composition and pressure, at room temperature. On the

other hand, we indicate with λ_z the moving resonance, as resulting from temperature changes. Optical bistability is effectively achieved by keeping the samples exposed to ethanol at pressure P close to the saturation point P_0 , while an optical beam—with spectrum centered at wavelength $\lambda_o \approx \lambda_{dry}$ —is incident onto the sample. At zero or low laser power, $\lambda_z \approx \lambda_{wet}$. The sample remains in a “low transmission state” (LTS) because the mismatch $\lambda_z - \lambda_o$ prevents significant penetration of light inside the sample. Thus, the sample remains in thermal equilibrium with the environment (its temperature stays equal to room temperature), and the mismatch remains large. Upon increasing the optical power, the optical absorption becomes large enough, leading to a temperature rise and to the evaporation of condensed ethanol. Evaporation causes a shift of λ_z toward the dry value λ_{dry} , leading to a lowering of the mismatch, to a larger absorption of optical power, and thus to a further temperature rise. Therefore, a positive feedback loop establishes. At a critical power level, the system becomes unstable and the central wavelength λ_z collapses to λ_{dry} . If $\lambda_{dry} \leq \lambda_o < \lambda_{wet}$, complete cancellation of the mismatch can be achieved. When λ_z reaches λ_o , the feedback becomes negative, “locking” λ_z to λ_o . Negative feedback occurs because the efficiency of optical power injection into the device is maximum at zero mismatch between λ_z and λ_o . Therefore, a further decrease of λ_z would decrease the power injection, the device would start cooling, and condensation would drive λ_z back toward λ_o .²⁶

The critical power at which the system becomes unstable is therefore the threshold power for switching to the “high transmission state” (HTS), which we term the low-to-high (P_{L-H}) threshold. Once in HTS, the transmission can be reset to LTS by lowering the incident optical power. This reversal occurs when the incident optical power crosses a high-to-low (P_{H-L}) threshold. When in LTS, the mismatch between the λ_z and λ_o makes the incident beam ineffective in injecting optical power inside the photonic structure and thus raising the system’s temperature. On the contrary, when in HTS, λ_z is “locked” to λ_o , thereby maximizing the power transfer from the beam to the sample. We note that the central wavelength λ_o of the optical beam must be carefully selected, depending on the porous material that is employed. On one side, there must be a significant absorption of light by the system, at wavelength λ_o , to control the temperature modulation. On the other hand, however, absorption must be sufficiently low to maintain good quality minibands and Wannier–Stark ladders. The guideline is to pick this wavelength inside the absorption band of the porous Si matrix but in proximity of the absorption band edge. We have chosen $\lambda_o = 973$ nm and fabricated the ZT structure with central dry wavelength $\lambda_{dry} = 967$ nm. Finally, we mention that if $\lambda_o \leq \lambda_{dry}$, bistability could still appear, but because of the residual mismatch in HTS, the modulation ratio between LTS and HTS would be reduced.

The bistability mechanism we have just described, being based on the spectral shift due to capillary condensation, is actually quite generally applicable to various porous photonic structures, including, in particular, single Fabry–Pérot microcavities. The ZT structure we are suggesting here is not necessarily the best for bistability. Compared to other structures, we expect that the ZT structure favors a wider hysteresis

in the transmission bistability, as the mechanism is based on detuning a resonant tunneling condition. However, this is at present just a conjecture and, therefore, it is an interesting opportunity for further investigation.

In the following, we focus on characterizing the bistability effect in time and as a function of concentration. This characterization is interesting not only for potential applications but also because it can give valuable information on the evaporation and condensation mechanisms of liquids inside mesoporous structures.

III. EXPERIMENTS

Mesoporous optical superlattices have been electrochemically etched into Boron doped (100)-oriented silicon substrates with a resistivity of 0.01–0.02 Ω cm. Room temperature anodization was performed using a solution of 30% volumetric fraction of aqueous HF (48 wt %) with ethanol.

The samples consisted of sequences of four different types of layers A to D , with different porosities and/or thicknesses. Layers A and B (the layers of the distributed Bragg reflectors) had an optical thickness of $\lambda/4$, where λ is the center of the stop band. C and D (the layers of the cavities) had optical thicknesses of $(\lambda - \Delta\lambda)/2$ and $(\lambda + \Delta\lambda)/2$, respectively, where $\Delta\lambda$ is the designed gap between the minibands. Layers C and D form half wavelength cavities which were alternated by Bragg mirrors formed by alternating A and B . The sample structure corresponded, therefore, to the sequence $BABABABCABABABDBABABABC, \dots$, etc.

The optical thickness of each layer depends both on its porosity and on its thickness. In turn, the porosity is controlled by the current density used during etching. Two current densities (50 and 7 mA/cm²) have been alternated to etch high and low porosity layers. The nominal porosities and the refractive indices were $p_A = p_C = p_D = 68\%$, $n_A \sim 1.45$ and $p_B = 50\%$, $n_B \sim 2.1$. Using silicon etch rates (ρ) for different current densities, the physical thicknesses d of the layers were controlled by the etch duration per layer, defined as $t_{etch} = d/\rho$, in order to achieve Zener tunneling structures centered at wavelength $\lambda_z = 967$ nm. The full structure consisted of 129 layers, leading to a total thickness of about 30 μ m.

To introduce the required optical thickness gradients, etch-stop current steps were used, which controlled the resulting refractive index and, therefore, the final optical thickness for each layer. Etch stops cause a partial chemical etching of the porous layer, which can be controlled by the etch-stop time. The longer a layer remains in contact with the electrolyte, the larger is the effect of the etch stops. The refractive index gradients were partially compensated by applying a linear gradient of layer thicknesses (via etch durations). Finally, the samples were made freestanding by applying an electropolishing current pulse of 0.32 A/cm² at the end of the growth process. The pore size within a monolayer of the superlattice presents a broad distribution [extracted from scanning electron microscopy (SEM) analysis] and for the cavity layers it ranges from 26 ± 10 nm at the low porosity side of the superlattice to 33 ± 10 nm at the high porosity side (average monolayer porosities of 68% and 76%).

We performed transmission measurements, in which an incident white light beam was focused on the superlattice,

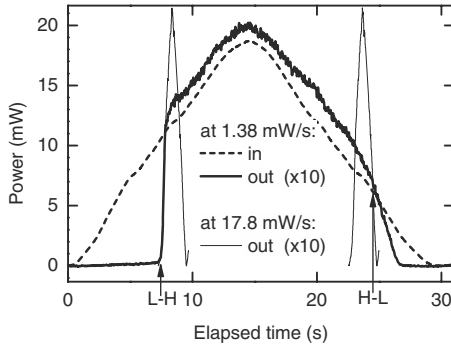


FIG. 3. Temporal profile of the power of incident (dashed line) and transmitted (solid thick line, with $10\times$ magnification) beams at slow sweeping speed, under exposure to 100% ethanol concentration. The transmitted beam at the highest sweep speed is also shown for comparison (solid thin line, shown twice to facilitate the visual comparison of the rising and falling fronts with the slow sweeping case).

collinearly with a laser pump beam. A fiber bunch collected the transmitted signals, which were sent to a spectrometer interfaced to a cooled charge coupled device. A flow of ethanol vapor was realized close to the sample surface using a gas-controller device.

For the transmission measurements, we selected as probe beam a laser whose wavelength $\lambda_o=973$ nm was close but slightly larger than the Zener tunneling peak. We focused the beam on a spot of $50\ \mu\text{m}$ diameter. During the experiment, we have continuously recorded the transmitted power while sweeping the incident power between 0 and 20 mW with triangular modulation, i.e., with constant and equal slopes, but opposite in sign for the rising and falling fronts. The slope was adjusted between 1.38 and 17.8 mW/s. The sample was exposed to a constant flux of air ($500\ \text{cm}^3/\text{min}$) at room temperature, containing ethanol vapor in adjustable amounts. The partial ethanol pressure (relative to saturation) was in the range between 76% and 100% (nominal values), as obtained by volumetric mixing of dry and saturated air in controlled fraction while keeping the total flux constant.

IV. TIME RESPONSE

In Fig. 3, we show the incident (“in”) and the transmitted (“out”) power versus time for the slowest sweep velocity (1.38 mW/s) and under maximum ethanol concentration (nominally 100%, i.e., at its dew point). We define a sweep as quasistatic when the complete curve of transmitted versus incident power is insensitive to further decrease of the sweeping speed, which was the case for the measurement of Fig. 3. In the first LTS (between 0 and 7.5 s in Fig. 3), the transmission is low because of the mismatch between the Zener wavelength $\lambda_z \approx \lambda_{wet}$ and the laser wavelength λ_o . When the incident power reaches the $P_{L-H} \approx 11$ mW threshold (at time ≈ 7.5 s), λ_z collapses to λ_o (locked state), the system switches to HTS, and the output starts to follow the input. At the other threshold $P_{H-L} \approx 6$ mW (time ≈ 24.5 s), the incident power becomes too low to maintain the locked state, condensation occurs, the locking mechanism is re-

leased, and the central wavelength λ_z switches back to its initial $\lambda_{wet} > \lambda_o$ value.

In Fig. 3, at first, it appears that the $L-H$ transition, which is associated with evaporation, is much faster than the $H-L$ transition, which is associated with condensation. A faster evaporation is also expected from previous results on microcavities.¹⁴ However, care must be taken to extract the switching times from Fig. 3. The $L-H$ transition dynamics is the result of a complex interplay between all phenomena involved in the collapse due to positive feedback and is essentially independent of the input sweep rate. This is evident by comparing the rise fronts of the transmission associated with 1.38 mW/s (slowest sweep) and 17.8 mW/s (fastest sweep) input powers. On the other hand, the $H-L$ transition is determined by a thermal relaxation mechanism.

The relaxation time constant τ of this thermal relaxation mechanism can be extracted from our data as follows. If we consider the dynamics of a single pore under ramped excitation, the Laplace transform of the transmitted beam $T(s)$ has the generic form¹⁵

$$T(s) = \frac{\tau A}{s^2} - \frac{\tau^2 A}{s} + \frac{\tau^3 A}{1 + s/\tau}, \quad (2)$$

where A is a constant that depends on the input rate. Therefore, the transmission signal in time is a linear combination of a ramp, a step function, and an exponential transient. The latter term becomes apparent only after switching events [in Eq. (2), the change of sign of the slope implies the change of sign of constant A]. We have extracted the exponential decay in correspondence of those transient regions and found decaying time constants 0.35 and 0.07 s, respectively, for the slow and fast sweeps. The relaxation time depends, therefore, clearly on the sweeping speed.

In Fig. 4, we show the transmission coefficient (the ratio between transmitted and incident powers) versus the incident power for six different sweeping rates. The incident power is repeatedly swept up and down with a triangular function, as described above. Except for the 1.38 mW/s rate, the measurements are not quasistatic. All measurements are, however, recorded once successive output cycles had become reproducible, which typically occurs after the second triangular cycle onward.

Figure 4 displays a remarkable modulation ratio by 2 orders of magnitude between the HTS and the LTS. The solid line without symbols (1.38 mW/s) originates from the same measurement as the data reported in Fig. 3. As we increase the sweep rate from 1.38 mW/s (solid line) to 3.92 mW/s (dashed line), we observe a shift to higher (lower) power of the rising (falling) arm. This shift is the result of a time lag of the switching events with respect to the quasistatic case, which leads to an opening of the hysteresis cycle. We are thus exiting the quasistatic regime already at 3.92 mW/s sweep rate. Upon further increasing the sweep rate (4.87 mW/s, diamond markers), we observe that the falling arm keeps the trend of opening the hysteresis, whereas the rising arm starts to “bounce” back toward lower powers. This can be understood as due to the incomplete thermalization of the liquid after the falling arm. At this sweeping speed, the falling arm barely reaches the LTS level before the incident

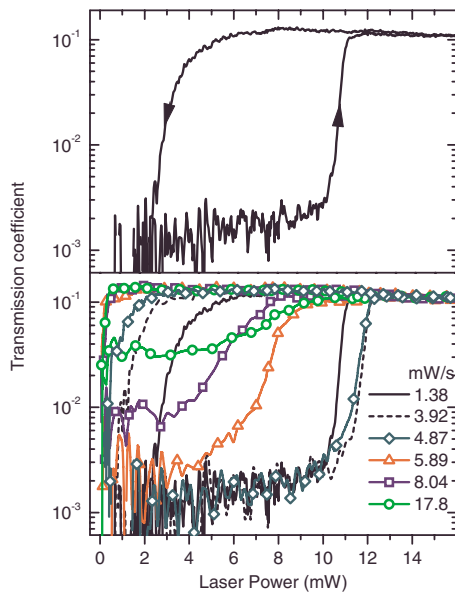


FIG. 4. (Color online) Ratio of the transmitted versus incident power as a function of the incident power. Ethanol is at nominal 100% concentration. Arrows indicate the direction of the measurement.

power starts to rise again. If we look at even faster rates, the falling arms does not fall all the way to the original low level. We thus conclude that at fast sweep rates, the limiting phenomenon is the condensation.

There is, however, a subtle additional feature. At a fast rate, the falling fronts accumulate as steep though incomplete transitions at 0 power. In other words, it seems that the speed-limiting phenomenon (condensation) gets *faster* at a faster sweeping speed. This is consistent with the previous observation (the behavior versus time) that the time constant of condensation depends on the sweeping speed. Moreover, upon the start of successive cycles, the transmission remains almost constant with rising input power, as if the condensation would get “pinned” to the level reached right before the sweep starts again. This behavior can be explained as follows. When the temperature rises, the critical radius r_c becomes smaller according to Eq. (1). After the L - H collapse, the pores are essentially empty and r_c is at its minimum. When the power decreases, the temperature drops, and the first pores which get filled are the smallest ones. These pores are also the fastest to thermalize, as they have the largest surface versus volume ratio. Then, if we stop the condensation process before it finishes, we essentially cut the largest—and therefore slowest—pores out of the dynamics. This explains why the relaxation time is also faster under a faster input sweep. The “pinning” effect is due to the interruption of the condensation, which leaves out the larger pores and blocks the spectral shift.

We finally discuss the factor of 5 in the difference between the relaxation times of 0.35 and 0.07 s, respectively, of the slowest (1.38 mW/s) and the fastest (17.8 mW/s) input sweep. According to the Fourier equation for heat transfer in the simplest approximation (cylindrical pores), we find that the thermalization time should be proportional to the

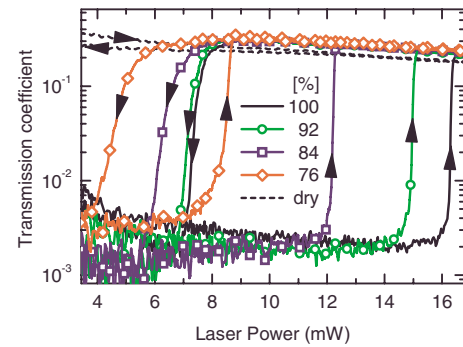


FIG. 5. (Color online) Ratio of the transmitted versus incident power as a function of the incident power. The nominal concentration of ethanol ranges from 76% to 100%, relative to its saturated vapor concentration at room temperature. Arrows indicate the sweep direction. Sweep speed is 1.38 mW/s. A control measurement with no vapor (dashed line, labeled as dry) is also reported. The sample of this measurement is not the same sample used in Figs. 3 and 4.

lateral surface versus the volume ratio, which is inversely proportional to the cylinder radius. However, from the SEM analysis of our samples, we find that there is only a factor of 3 between the radii of largest and smallest pores.²³ The difference between the decay time constants can, however, be larger than the prediction from geometrical arguments because of an additional limiting effect in the gas diffusion process. When condensation starts to fill the smallest pores, the porous network becomes less percolating (regions of pores filled with liquid become “clogged”), which makes it harder for the ethanol gas to reach inside the larger pores.²⁵

V. CONCENTRATION EFFECTS

In Fig. 5, we show the transmission coefficient versus the incident power for four different concentrations. Measurements at the sweep speed (1.38 mW/s) are all quasistatic with this sample.

The control measurement in Fig. 5, labeled as “dry,” is obtained without vapor. The sample was fabricated with a transmission band almost matching the input beam when in dry condition ($\lambda_{dry} \approx \lambda_o$). Hence, the transmission of the dry sample is expected to be essentially constant and high, under any pumping condition, which is what we indeed observe experimentally. Note that the transmission for the dry sample is slightly lower than the HTS in presence of vapor. This is because—under vapor exposure—the transmission is maximized by the “locking effect” discussed previously.

We observe from the measurements that both the thresholds P_{L-H} and P_{H-L} decrease with the concentration. The P_{L-H} threshold decreases because, at equal temperature, a lower concentration implies a smaller critical radius [Eq. (1)], a less condensed liquid, and a smaller $\lambda_c - \lambda_o$ mismatch. This means that the input beam injects more energy already from the beginning of the sweep, and the sample gets heated more effectively. Hence, the power threshold to trigger the L - H jump is lower. On the other hand, as seen from Eq. (1), when we decrease the power from the sample in the HTS to reach

a certain critical radius, the lower the concentration, the more the temperature must be decreased. Therefore, P_{H-L} also decreases.

By looking at Eq. (1), we observe that the sensitivity of the critical radius to the vapor pressure ($\partial r_c / \partial P$) is larger for concentrations in proximity of the saturation point P_0 . From Fig. 5, however, we see that the sensitivity of the thresholds to the pressure is larger at $P/P_0=76\%$ than $P/P_0=100\%$. To explain why the upper threshold P_{L-H} is not very sensitive to concentration at high concentration values, one must consider the interplay of two factors. First, at high concentration, the spectral mismatch is large. The overlap between the spectrum of the Zener band and the laser is therefore poor, which results in inefficient heating regardless of the precise value of the Zener wavelength λ_z . Second, the range of pore sizes is finite ($r_{min} \leq r \leq r_{max}$); thus, when $P \geq P_0 \exp(-v_m \gamma / Tr_{max})$, the pores are essentially all filled [Eq. (1)] regardless of the exact value of P .

VI. CONCLUSIONS

We have reported a detailed analysis of the bistability effect of optical transmission in a one-dimensional photonic structure exhibiting a narrow transmission band based on optical Zener tunneling. The photonic structure is a porous

matrix, which is exposed to ethanol vapor during the experiments. By condensing inside the pores, the vapor modulates the effective refractive index of the structure and leads to spectral shifts and to bistability. A hysteresis cycle appears in the transmission versus incident power as a consequence of an intricate feedback mechanism. The two bistable levels of optical transmission differ by factor as large as 2 orders of magnitude.

We have characterized the dependence of the hysteresis loop on the sweeping rate and on the vapor concentration. In the latter case, we have run experiments in the quasistatic regime and showed a dependence of the switching thresholds on the vapor concentration that is qualitatively consistent with a nontrivial interplay of the Kelvin equation and the modulation of optical spectra overlap. In the first case, on the other hand, we have also investigated the effect of taking the system out of the quasistatic regime. This implies a compression of the hysteresis loop toward the high transmission state, i.e., the state for which the liquid is partially removed by heating. This compression indicates that condensation rather than evaporation is the speed-limiting bottleneck of the system. We have also shown that the condensation dynamics is faster in pores with lower radius, a feature which is consistent with the thermal exchange being controlled by the surface versus volume ratio of pores.

-
- ¹D. W. Prather, S. Shi, J. Murakowski, G. J. Schneider, A. Sharkawy, C. Chen, and B. Miao, *IEEE J. Sel. Top. Quantum Electron.* **12**, 1416 (2004).
- ²V. R. Almeida, C. A. Barrios, R. R. Panepucci, and M. Lipson, *Nature (London)* **431**, 1081 (2004).
- ³C.-S. Kee and H. Lim, *Phys. Rev. B* **64**, 121103(R) (2001).
- ⁴K. Busch and S. John, *Phys. Rev. Lett.* **83**, 967 (1999).
- ⁵H. Takeda and K. Yoshino, *Phys. Rev. E* **67**, 056607 (2003).
- ⁶A. Figotin, Y. A. Godin, and I. Vitebsky, *Phys. Rev. B* **57**, 2841 (1998).
- ⁷W. M. Lee, P. M. Hui, and D. Stroud, *Phys. Rev. B* **51**, 8634 (1995).
- ⁸C. H. Raymond Ooi, T. C. Au Yeung, C. H. Kam, and T. K. Lim, *Phys. Rev. B* **61**, 5920 (2000).
- ⁹H. Takeda and K. Yoshino, *Phys. Rev. B* **67**, 245109 (2003).
- ¹⁰W. Thompson, *Proc. R. Soc. Edinburgh* **7**, 63 (1870).
- ¹¹W. Theiß, *Surf. Sci. Rep.* **29**, 91 (1997).
- ¹²D. A. G. Bruggeman, *Ann. Phys.* **24**, 636 (1935).
- ¹³R. B. Bjorklund, S. Zangoie, and H. Arwin, *Appl. Phys. Lett.* **69**, 3001 (1996).
- ¹⁴Z. Gaburro, N. Dalosso, L. Pavesi, G. Faglia, C. Baratto, and G. Sberveglieri, *Appl. Phys. Lett.* **78**, 3744 (2001).
- ¹⁵See, for example, J. L. Schiff, *The Laplace Transform Theory and Applications* (Springer, New York, 1999).
- ¹⁶M. Ghulinyan, Z. Gaburro, D. S. Wiersma, and L. Pavesi, *Phys. Rev. B* **74**, 045118 (2006).
- ¹⁷T. Ikeda, *J. Mater. Chem.* **13**, 2037 (2003).
- ¹⁸B. E. A. Saleh and M. C. Teich, *Fundamentals of Photonics* (Wiley, New York, 1991).
- ¹⁹H. W. Tan, H. M. van Driel, S. L. Schweizer, R. B. Wehrspohn, and U. Gösele, *Phys. Rev. B* **70**, 205110 (2004).
- ²⁰A. Hache and M. Bourgeois, *Appl. Phys. Lett.* **77**, 4089 (2000).
- ²¹M. Notomi, A. Shinya, S. Mitsugi, G. Kira, E. Kuramochi, and T. Tanabe, *Opt. Express* **13**, 2678 (2005).
- ²²M. Chen, C. Li, M. Xu, W. Wang, Y. Xia, and S. Ma, *Opt. Commun.* **255**, 46 (2005).
- ²³P. Barthelemy, M. Ghulinyan, Z. Gaburro, C. Toninelli, L. Pavesi, and D. Wiersma, *Nat. Photonics* **1**, 172 (2007).
- ²⁴M. Ghulinyan, C. J. Oton, Z. Gaburro, L. Pavesi, C. Toninelli, and D. S. Wiersma, *Phys. Rev. Lett.* **94**, 127401 (2005).
- ²⁵D. Wallacher, N. Künzner, D. Kovalev, N. Korr, and K. Knorr, *Phys. Rev. Lett.* **92**, 195704 (2004).
- ²⁶If $\lambda_o \leq \lambda_{dry}$, λ_z cannot reach λ_o since λ_{dry} is the minimal reachable value. In such case, the mismatch cannot be fully canceled.